Turkish Journal of Chemistry

Volume 46 | Number 3 Article 25

1-1-2022

Microstructure and ionic conductivity investigation of samarium doped ceria(Sm0.2Ce0.8O1.9) electrolytes prepared by the templating methods

DİLARA GÜÇTAŞ

VEDAT SARIBOĞA

MEHMET ALİ FARUK ÖKSÜZÖMER

Follow this and additional works at: https://journals.tubitak.gov.tr/chem

Part of the Chemistry Commons

Recommended Citation

GÜÇTAŞ, DİLARA; SARIBOĞA, VEDAT; and ÖKSÜZÖMER, MEHMET ALİ FARUK (2022) "Microstructure and ionic conductivity investigation of samarium doped ceria(Sm0.2Ce0.8O1.9) electrolytes prepared by the templating methods," *Turkish Journal of Chemistry*: Vol. 46: No. 3, Article 25. https://doi.org/10.55730/1300-0527.3379

Available at: https://journals.tubitak.gov.tr/chem/vol46/iss3/25

This Article is brought to you for free and open access by TÜBİTAK Academic Journals. It has been accepted for inclusion in Turkish Journal of Chemistry by an authorized editor of TÜBİTAK Academic Journals. For more information, please contact academic.publications@tubitak.gov.tr.

TÜBİTAK

Turkish Journal of Chemistry

http://journals.tubitak.gov.tr/chem/

Research Article

Turk J Chem
(2022) 46: 910-922
© TÜBİTAK
10.55730/1300-0527.3379

Microstructure and ionic conductivity investigation of samarium doped ceria ($Sm_{0.2}Ce_{0.8}O_{1.9}$) electrolytes prepared by the templating methods

Dilara GÜÇTAŞ, Vedat SARIBOĞA, M.A. Faruk ÖKSÜZÖMER*
Department of Chemical Engineering, Faculty of Engineering, İstanbul University-Cerrahpaşa, İstanbul, Turkey

Received: 17.11.2021 • **Accepted/Published Online:** 25.02.2022 • **Final Version:** 16.06.2022

Abstract: $Sm_{0.2}Ce_{0.8}O_{1.9}$ (SDC20) electrolytes were synthesized with cellulose templating (CT) and PVA templating (PVAT) methods. Powder characteristics were examined using TG/DTA, XRD, and SEM. Pellets are sintered at various temperatures for different durations. Mean grain sizes were calculated from SEM micrographs using the linear intercept method. Grain growth behavior of the electrolytes was investigated and the dominant diffusion mechanism was examined. The grain growth activation energies were obtained for the first time for the mentioned electrolytes prepared by the mentioned methods. The ionic conductivities were calculated by electrochemical impedance spectroscopy. The highest ionic conductivity value was found to be 0.050 S cm^{-1} for the cellulose templating method.

Key words: SOFC, electrolyte, SDC20, sintering, grain growth, templating

1. Introduction

Solid oxide fuel cells (SOFCs) are recognized as the most effective energy conversion devices with future applications. Lowering the operating temperature of SOFCs is extremely important for efficient operation [1]. This can be achieved by using the effective electrolyte under the right conditions. The ionic conductivity of the electrolyte is the most crucial aspect affecting the efficiency of solid oxide fuel cells. The electrolyte is responsible for ion transport within the cell to create electrochemical reactions. Numerous chemical materials are reported in the literature as the best electrolyte for SOFCs, but among all the doped ceria compounds show outstanding performance due to their specific properties, such as low activation energy in the 500–800 °C temperature range [2]. The ionic conductivity is highly affected by the concentration and the ionic radius of the dopant cations. Among the various dopants used, Sm^{3+}, and Gd^{3+} are favorable for increasing the ionic conductivity [3].

There are many methods reported to prepare doped ceria compounds such as coprecipitation methods by using precipitation agents like ammonium hydroxide [4], oxalic acid [5], and ammonium carbonate [6], or auto-combustion methods using fuels such as citric acid [7], glycine [8], ethylene glycol [9], and EDTA [10]. Additionally, templating methods provide extremely pure and fine particle-sized ceramic powders. In this method, metal cations are prepared in solution and trapped in a template. The template burns out with calcination and, the resulting combustion heat contributes to the crystallization of the obtained ceramic. Compounds such as chitosan, polyvinyl alcohol, and cellulose can be used as templates for the production of SDC20 electrolytes. [11–13].

Another crucial parameter to achieve high-performance electrolytes is considered the sintering process. Sintering at high temperatures is essential to achieve a dense, nonporous structure. Knowing the effective sintering temperature and time is extremely important in terms of efficiency, time, and cost.

The ionic conductivity is affected by the electrolyte's grain size after sintering. In general, the grain size of ceramics increases as the sintering temperature increases. The grain growth of the electrolyte is usually controlled by grain boundary diffusion and lattice diffusion. The dominant mechanism during sintering significantly affects the properties of the final product.

Studies on grain growth kinetics of SDC20 are quite limited in the literature. The most detailed study was carried out by our group using the chitosan templating method. In our work, the dominant grain growth mechanism during sintering was determined by sintering SDC20 electrolytes at different temperatures [14].

In this work $Sm_{0.2}Ce_{0.8}O_{1.9}$ (SDC20) electrolytes were synthesized by the cellulose templating and polyvinyl alcohol (PVA) templating methods. Samples were sintered at 1200, 1300, and 1400 °C for 5 min, 1 h, and 6 h each. The grain

* Correspondence: fufu@iuc.edu.tr

This work is licensed under a Creative Commons Attribution 4.0 International License.

sizes of the electrolytes were determined and the relationship between the synthesis method and sintering kinetics was investigated for the first time to the best of our knowledge.

2. Materials and methods

SDC20 ($Sm_{0.2}Ce_{0.8}O_{1.9}$, SDC20) electrolytes were synthesized according to the CT and PVAT methods reported in the literature [15,16].

2.1. Cellulose templating method

$Ce(NO_3)_3.6H_2O$ (Alfa Aesar, 99.5%), $Sm(NO_3)_3.6H_2O$ (Alfa Aesar, 99.9%) were dissolved in water and 1 M solution was prepared. Then, the solution was dropped onto 125 mm diameter ashless cellulose filter paper (Macharey-Nagel, MN 640 de, ≤2 μm) in the ratio of 1 mL solution per filter paper. Afterward, the penetrated cellulose papers were burned in a preheated oven (500 °C) for 30 min and then calcined at 600 °C for 6 h. The remaining foamy residue (Figure 1) consists of pure metal oxides. Then, the residue ground in an agate mortar and pure SDC20 powders were obtained.

2.2. PVA templating method

A total of 0.5 M cation solution was prepared by dissolving $Ce(NO_3)_3.6H_2O$ (Alfa Aesar, 99.5%) and $Sm(NO_3)_3.6H_2O$ (Alfa Aesar, 99.9%) in distilled water in the correct stoichiometric amounts. Subsequently, an aqueous PVA (5 wt.%) solution was prepared and added to the cation solution with the molar ratio of PVA to cations P: C = 1. Then, a homogeneous solution was obtained by mixing the solution for 48 h. Afterward, the solution was poured into a flat surface and left to dry at room temperature for 4 days, and a clear and flexible film (Figure 2) was obtained. The calcination of the precursor was carried out at 600 °C for 6 h and the resulting foamy material was ground in an agate mortar.

The ceramic powders were pressed into 10 mm diameter pellets via stainless steel pellet die. To increase their strength, cold isostatic press was applied. Later, pellets were sintered at 1200–1400 °C temperature range for 5 min, 1 h, and 6 h with a 5 °C/min heating rate.

The thermogravimetric analysis was applied to the precursors prior to calcination with Seiko SII Exstar 6000 thermogravimetric/differential thermal analysis between 30 °C and 800 °C.

XRD analysis was applied to the samples to explore the crystalline structure. The powders after calcination and the powders of ground pellets were studied by XRD using Rigaku D/max-2200 diffractometer with CuKα radiation in an angular region of $2\theta = 20°– 80°$.

The theoretical densities were calculated by Equation (1), and the sample densities were measured using the Archimedes method.

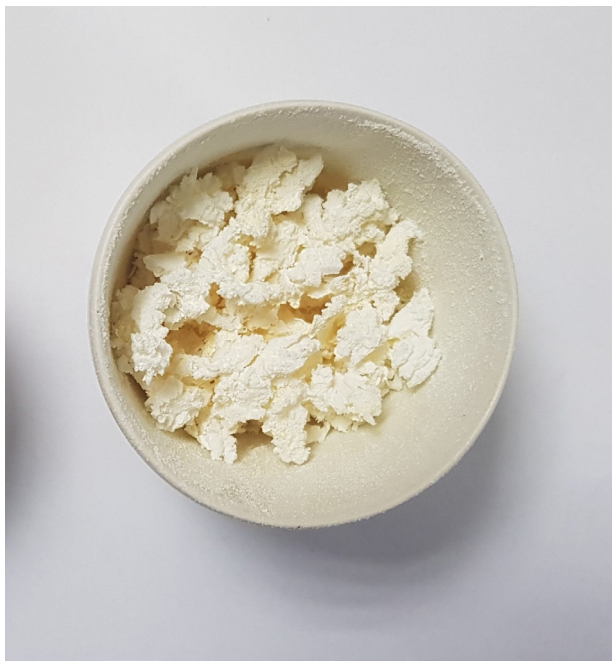

Figure 1. The foamy SDC20 ceramic structure after calcination.

$$\rho = \frac{[xM_d + (1-x)M_{Ce} + \left(2-\frac{x}{2}\right)M_O]}{N_A a^3} \quad (1)$$

where ρ is the theoretical density (g cm^{-3}),

x is the dopant concentration,

M_d is the molecular weight of the dopant,

M_{Ce} is the molecular weight of the cerium,

M_O is the molecular weight of the oxygen,

a is the lattice parameter, and

N_A is the Avogadro number.

Microstructural properties of the sintered electrolytes were investigated via scanning electron microscope (SEM-EDX, FEI Quanta FEG-450). The average grain size of the electrolytes was calculated using the SEM micrographs, via the linear intercept method from three different micrographs. Then, a line through the micrograph was drawn, and the number of grain boundaries intersecting the line was counted. By dividing the number of intersections by the real line length, the mean grain size of the electrolytes was calculated. The estimation of the mean grain size of the electrolytes using only one micrograph is given in Figure 3. This process is repeated 3 times for all samples.

Figure 2. Clear and flexible PVA-cation film.

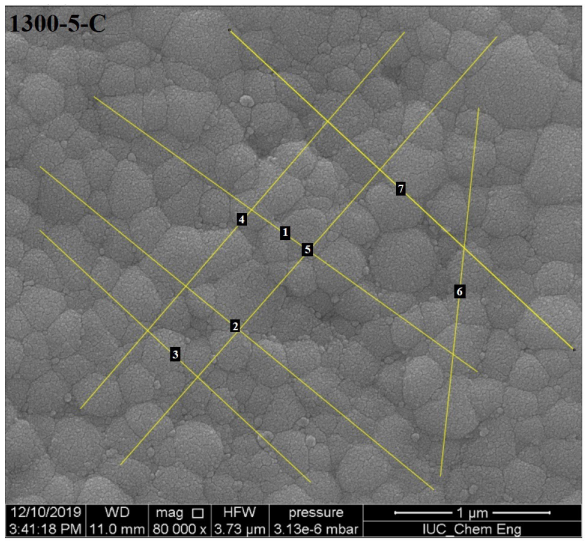

Line	Length (nm)	Number of Intercept	Grain Size (nm)
1	3086	14	220.43
2	3335	15	222.33
3	2420	12	201.67
4	3250	15	216.67
5	3734	19	196.53
6	2426	11	220.55
7	3081	13	237.00

Mean Grain Size = 216.5 nm

Figure 3. The linear intercept method for the mean grain size calculation.

Electrical properties of the electrolytes were measured by using a GAMRY Instruments PCI4G750/46070 Potentiostat in the 250-800 °C temperature range. The Nyquist curves were plotted and, the sample resistances (R) were obtained. Then, the total ionic conductivities of the samples were calculated using the equation below.

$$\sigma_{total} = \frac{l}{A.R_{total}} \quad (2)$$

where σ_{total} is the total ionic conductivity,
A is the crosssectional area of the sample
l is the sample thickness, and
R_{total} is the total resistance.

3. Results

3.1. Powder characterization

The thermal behavior of the both precursors prior to calcination were investigated with TG/DTA and the charts are given in Figures 4a and 4b.

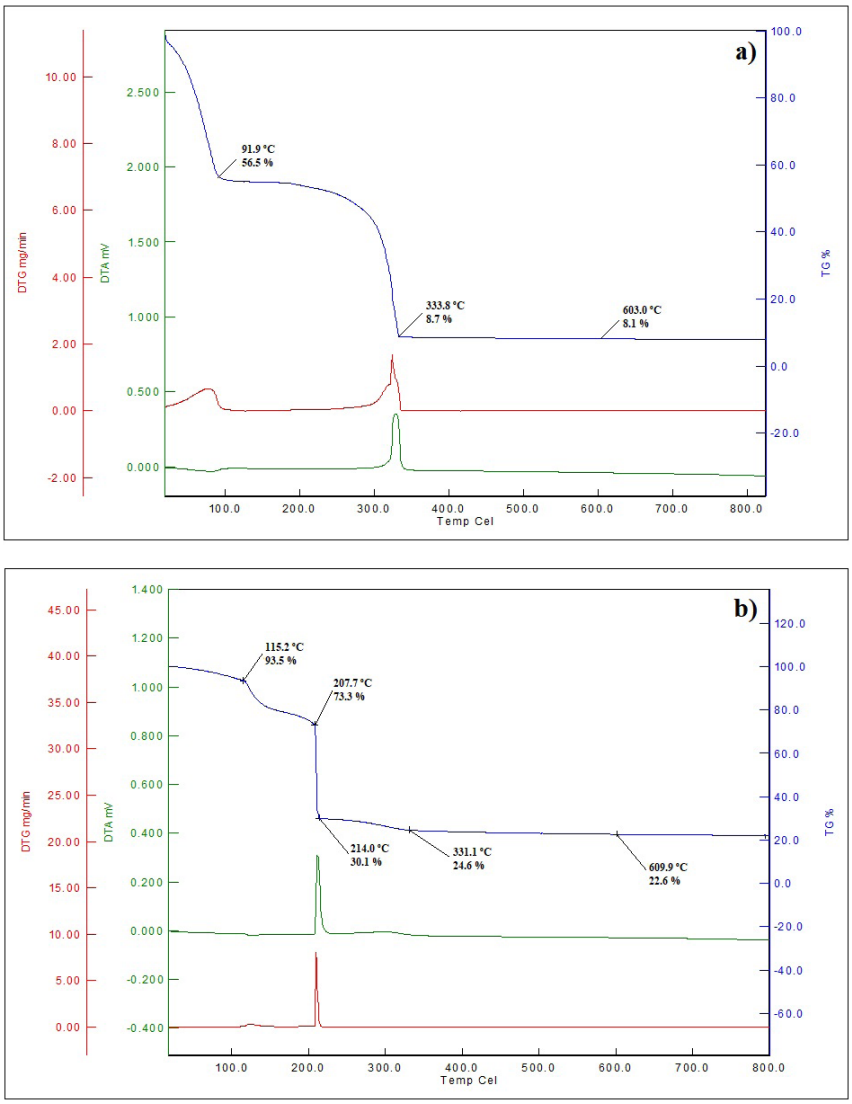

Figure 4. TG/DTA graph of the powders; (a) prepared by CT method, (b) prepared by PVAT method.

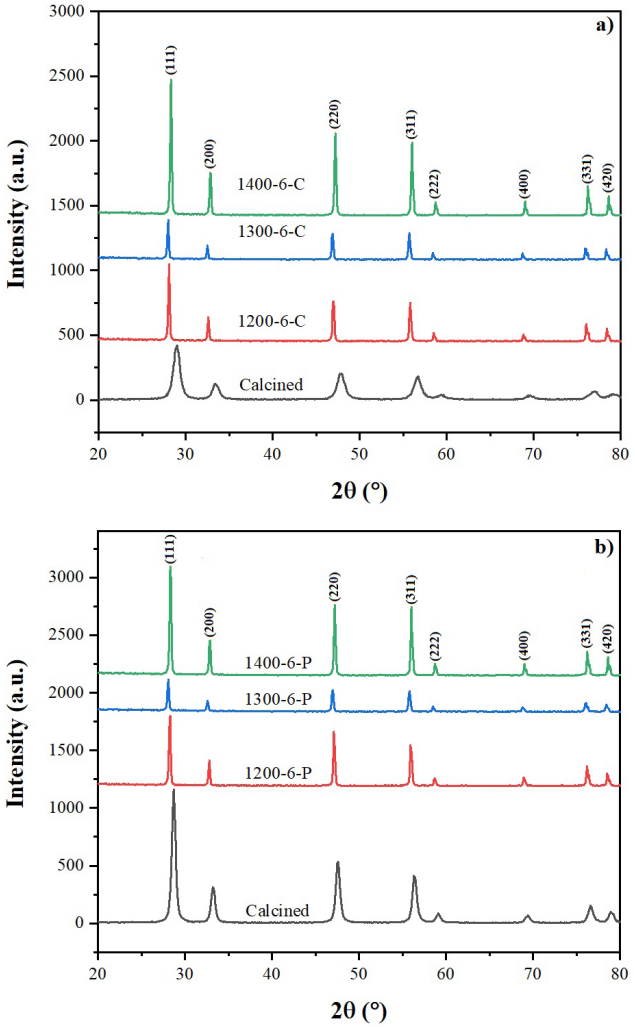

Figure 5. XRD patterns of the electrolytes after calcination and sintering a) prepared by CT method, b) prepared by PVAT method.

Figure 4a shows the TG/DTA results of the cation impregnated filter paper. The first weight loss (about 40%) resulted from the evaporation of the water. Then, a weight loss of 47% occurred at 333 °C and, SDC20 was obtained. Although the decomposition of the filter paper itself occurs at around 500 °C, the presence of the cations lowered the decomposition temperature and made it possible to form pure SDC20 in a single step. A small mass loss of 0.6% was observed until 600 °C and, the remaining mass can assume to be SDC20.

Figure 4b shows the TG/DTA results of the PVA-cation film. The initial weight loss of 6.5% may be attributed to the evaporation of the moisture in the film. Then, at 115 °C the decomposition of the PVA started. A sudden weight loss of 43% occurred and, SDC20 formed in the temperature range of 207–214 °C. Normally, the decomposition of pure PVA starts at 240 °C [17], but the presence of the cations lowered the decomposition temperature. The combustion of organic residues continued up to 330 °C and, about 2% of weight loss was observed until 600 °C. No remarkable weight loss was detected after this temperature and both powders were calcined at this temperature.

XRD patterns of the samples calcined at 600 °C and sintered at 1200, 1300, and 1400 °C for 6 h are given in Figure 5. XRD results show that crystallization of the powders occurred after calcination at 600 °C. The samples consist of single-phase CeO_2 with a cubic fluorite structure (JCPDS Card No: 34-394). No peak of samarium oxide was observed which shows the dopant cation was entirely placed in the lattice. The electrolytes are named to state the synthesis route and, sintering condition applied. For example, 1200-6-C refers to the sample synthesized by the CT method and sintered at 1200 °C for 6 h.

CT method includes penetration of cation solution inside the pores of the cellulose paper. The cellulose paper has a tightly packed structure with a low void volume. When the cerium-samarium solution has penetrated the pores and burned at 500 °C, the mixture of decomposed compounds created and was trapped in the cellulose paper [11]. Figure 6a shows SEM image of SDC20 powders after the filter paper is burned out. After burning the filter paper there is a networked fiber structure of Sm-Ce-O mixture, which consists of many mesh-like regions. On the other hand, the PVAT method includes the dopants incorporated into the ceria lattice via combustion for pure phase evolution [16]. Figure 6b shows SEM image of SDC20 powders after the calcination of the PVA-cation film and, the structure consists of sponge-like regions due to the release of large amounts of gases during calcination.

3.2. Sintering and microstructure

Figure 7 shows SEM micrographs of the electrolytes sintered at 1400 °C for 5 min, 1 h, and 6 h.

The samples prepared by both methods reached a dense and nonporous structure at 1400 °C, independent of the sintering time. However, it could be seen that the samples prepared with the cellulose templating method are denser

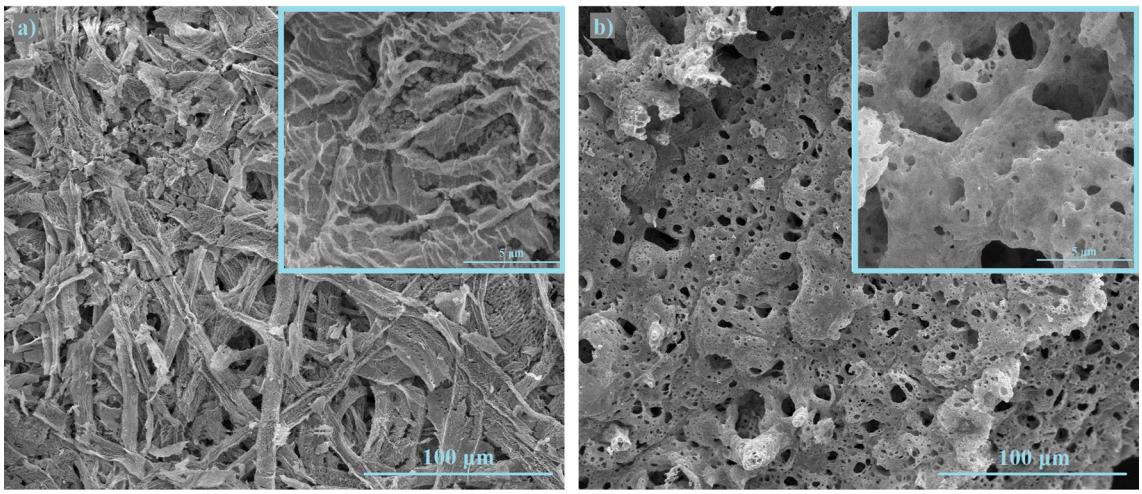

Figure 6. SEM micrographs of the powders; (a) prepared by CT method, (b) prepared by PVAT method.

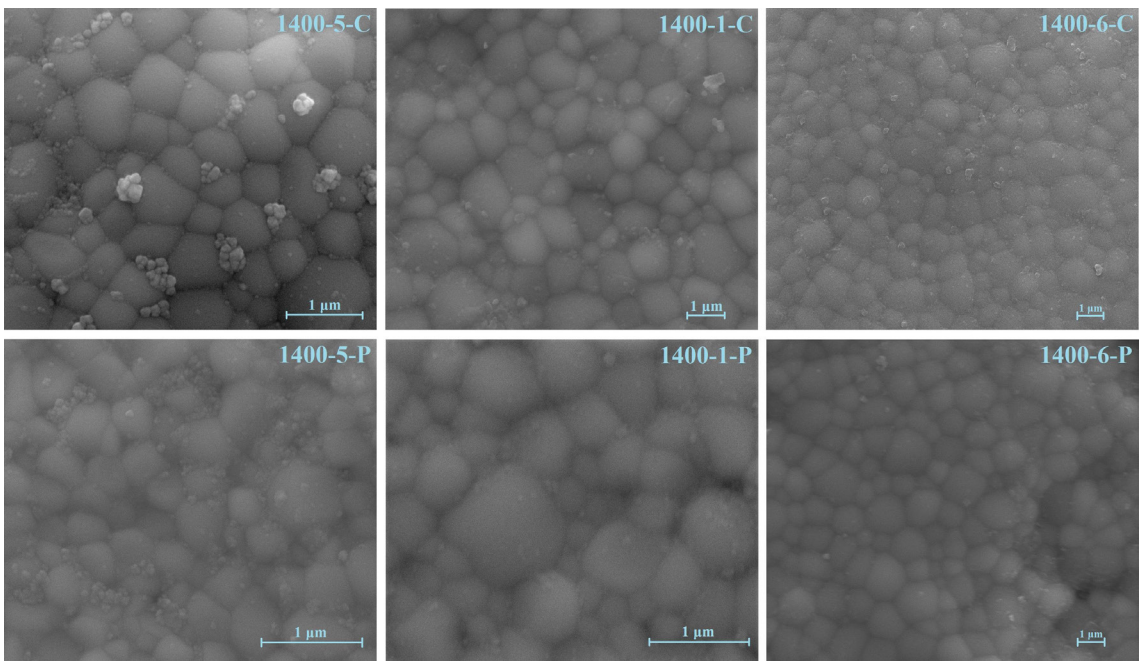

Figure 7. SEM micrographs of the pellets.

than the ones prepared with PVA templating method. At 1400 °C, the grains can be clearly distinguished and reached a hexagonal structure, regardless of the sintering time. Increasing the sintering time allowed the grains to grow noticeably. Longer sintering times are required to ensure homogeneous grain size distribution.

Density measurements of the sintered pellets were measured via the Archimedes method and all density values are given in Table 1.

For both methods, an increase in the sintering temperature gives higher density values. A relative density value greater than 88% was achieved under all sintering conditions. The samples prepared by the CT method have greater measured and relative density values than the samples prepared by PVAT method. Also, the densest material was the 1400-6-C sample, which was produced by the CT method and sintered at 1400 °C for 6 h. Although the highest density is achieved by sintering at 1400 °C for 6 h, it is possible to achieve comparable densities by sintering at 1300 °C. This means great advantage in terms of time and energy consumption for SDC20 materials.

Detailed grain growth analysis for polycrystalline structures is difficult due to the change of grain boundary energy which causes a change in the grain growth kinetic from boundary to boundary. To simplify the grain growth kinetic, grain boundary energy is presumed to be constant, and the grain growth kinetics can be explained with the following equations:

$$D^n - D_0^n = Kt, \tag{3}$$

$$K = K_0 e^{-\frac{Q}{RT}} \tag{4}$$

where D expresses the average grain size of the electrolyte,

D_0 is the grain size of the initial polycrystalline powders at the time (t = 0),

Q is the activation energy of grain growth,

K_0 is the rate constant,

t is the time, and

n is an exponent, which is an integer ranging from 1 to 4 depending on various kinetic parameters involved in the growth process [18].

Table 1. Measured, theoretical, and relative densities.

Sample	Measured density (g cm^{-3})	Theoretical density (g cm^{-3})	Relative density (%)
1200-5-C	6.31	7.14	88.35
1200-1-C	6.49	7.14	90.99
1200-6-C	6.68	7.12	93.75
1300-5-C	6.45	7.12	90.59
1300-1-C	6.66	7.12	93.58
1300-6-C	6.71	7.10	94.38
1400-5-C	6.66	7.12	93.51
1400-1-C	6.81	7.14	95.38
1400-6-C	6.89	7.14	96.58
1200-5-P	6.32	7.14	88.57
1200-1-P	6.42	7.14	89.99
1200-6-P	6.45	7.14	90.33
1300-5-P	6.41	7.12	90.03
1300-1-P	6.47	7.12	90.91
1300-6-P	6.49	7.12	91.17
1400-5-P	6.46	7.12	90.73
1400-1-P	6.57	7.14	92.07
1400-6-P	6.64	7.14	93.02

Sintering occurs through different diffusion mechanisms. The value of n changes according to the dominant diffusion mechanism. If n = 3, then the volume diffusion is dominant during sintering. If n = 4 then, the grain boundary diffusion is dominant [19].

The grain size of the starting powder (D_0) is quite small opposed to the electrolytes grain size (D), so D_0 can be neglected and, Equation (3) can be simplified as follows:

$$\frac{D^n}{t} = K_0 e^{-\frac{Q}{RT}} \tag{5}$$

If the same equation written in logarithmic scale:

$$ln\frac{D^n}{t} = lnK_0 - \frac{Q}{RT} \tag{6}$$

The grain growth exponent (n) can be estimated via the slope of the ln(D) – ln(t) plot if the activation energy is considered constant. Then, using Equation (6), it is possible to estimate the activation energy.

The average grain size of the electrolytes was calculated using the linear intercept method and given in Table 2. The highest grain size values for CT and PVAT methods are 1066.8 ± 10.4 nm and 1074.7 ± 8.1 nm, respectively. Both values are achieved after sintering at 1400 °C for 6 h. The lowest grain sizes for both methods at the same order are 122.2 ± 3.7 nm and 145.7 ± 3.0 nm. These values were achieved for 5 min sintering at 1200 °C. Increasing the sintering temperature caused the grain size to increase monotonically. Also, longer sintering times increase the average grain size of the electrolytes, but this increase is not linear with time.

Figure 8 represents the change of the average grain sizes with sintering conditions. The grain growth at 1200 °C showed an almost linear increase with sintering time. At 1300 °C and 1400 °C, as a result of increasing the sintering time from 5 min to 1 h, an increase of 1.5–2 times in the grain sizes was observed. Similarly, when the sintering time is increased to 6 h, an increase of 1.5 times is observed. This shows the grain growth is limited at a certain point as in our previous work [14].

The grain growth exponent "n" was calculated using Equation (6) and the dominant diffusion mechanism during sintering was determined. Figure 9 shows the lnD – lnt plot of the samples. The slope of this plot gives the value of 1/n. For all samples produced by both methods, the n = 4 was calculated. That shows the grain boundary diffusion is the dominant mechanism during the sintering of the electrolyte. The driving force for sintering comes from the defective structure of the grain boundaries. The lattice diffusion occurs slower than the grain boundary diffusion. Also, the grain boundary diffusion contributes more to the densification of the electrolyte rather than grain growth [20].

The sintering activation energies of the samples were calculated using Equation (6). Figure 10 shows Arrhenius plot of lnD^4/t – 1/T. The calculated activation energies are given in Table 3. For the samples prepared by the CT method, the sintering activation energies are calculated as 484.2, 591.9, and 453.9 kJ mol^{-1} for 5 min, 1 h, and 6 h of sintering, respectively. The sintering activation energies of the samples prepared by the PVAT method are calculated as 367.5, 391.3, and 275.5 kJ mol^{-1} for 5 min, 1 h, and 6 h of sintering, respectively. There is no recorded sintering activation energy for SDC20 synthesized by the CT and the PVAT methods in the literature. However, the activation energy of sintering was found to be 474.4 kJ mol^{-1} for the chitosan templating method [14]. Also, similar values have been noted for other oxide electrolytes such as 669 kJ mol^{-1} for $La_{0.8}Sr_{0.2}Ga_{0.83}Mg_{0.17}O_{2.815}$ [21], 697 kJ mol^{-1} for CeO_2 [22], 580 kJ mol^{-1} for yttria-stabilized zirconia [23].

Table 2. Mean grain sizes of all samples.

Sample	Mean grain size (D, nm)		
	5 min	**1 h**	**6 h**
1200 - C	122.2 ± 3.7	189.8 ± 4.7	351.5 ± 5.0
1300 - C	213.3 ± 2.9	392.6 ± 7.0	598.9 ± 9.0
1400 - C	399.5 ± 5.0	706.3 ± 10.2	1066.8 ± 10.4
1200 - P	145.7 ± 3.0	208.7 ± 5.3	423.7 ± 5.2
1300 - P	190.3 ± 3.6	343.2 ± 7.0	495.6 ± 5.7
1400 - P	360.4 ± 5.1	542.5 ± 7.9	1074.7 ± 8.1

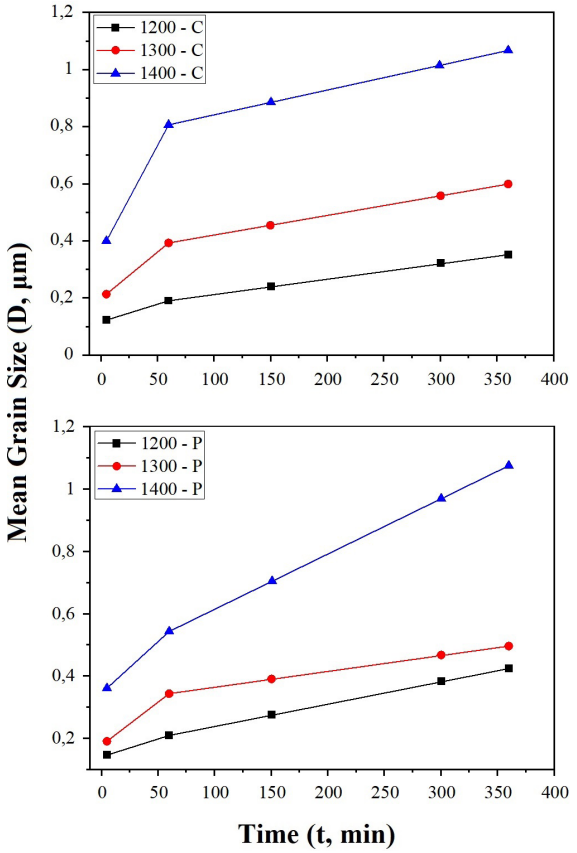

Figure 8. The effect of sintering conditions on the mean grain size.

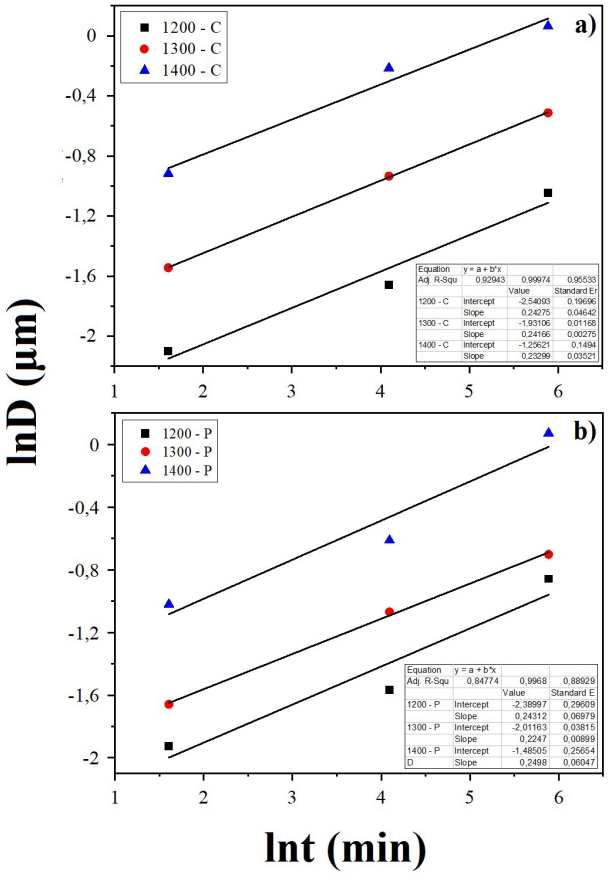

Figure 9. lnD-lnt plot for a) CT method, b) PVAT method.

3.3. Conductivity measurements

The electrical properties of the samples were determined by electrochemical impedance spectroscopy (EIS). Impedance measurements were applied to samples sintered at 1400 °C for 6 h. Figure 11 represents the impedance spectra measured at 800 °C for CT and PVAT samples. At this temperature, the total ionic conductivity of the sample prepared by the CT method was much higher (0.050 S cm^{-1}) than the sample prepared by the PVAT method (0.037 S cm^{-1}). This difference between the two samples also agrees with the SEM and density analysis considering the PVAT method results in a less dense structure. In this case, it was concluded that using cellulose as a templating agent against PVA gives better results.

Since the CT method gives better results, EIS analysis also applied the samples sintered at 1200 and 1300 °C, and the impedance spectra are given in Figure 12. The total conductivity values, area specific resistivity (ASR) values, and activation energies are given in Table 4. Specific resistance is the inherent property of a material. It is defined as the resistance offered per unit length and unit crosssectional area of the electrolyte when a known quantity of voltage is applied at its end. The reciprocal of the specific resistance gives the conductivity. Samples sintered at 1200 and 1300 °C have almost the same conductivity values which are 0.030 and 0.033 S cm−1, respectively, but at 1400 °C the total conductivity increased significantly.

Jaiswal et al. [24] calculated the ionic conductivity of SDC20 synthesized via auto-combustion method at 1350 °C as 0.0133 S cm^{-1}. Spiridigliozzi et al. [25] reported the ionic conductivity as 0.048 S cm^{-1} at 1300 °C for the coprecipitation route. Ma et al. [12] calculated the conductivity as 0.033 S cm^{-1} at 1300 °C for the PVAT method. Özdemir et al. [15] estimated the ionic conductivity of SDC20 as 0.031 S cm^{-1} at 1200 °C for the CT method. This study has proved that both cellulose templating and PVA templating methods are more effective than other methods in the literature for preparing high-performance SDC20 electrolytes.

Figure 13 shows the temperature dependence of the sample conductivities. The Arrhenius plots appear linear but they consist of two regions named LT (low temperature) and HT (high temperature) according to the change of the linearity

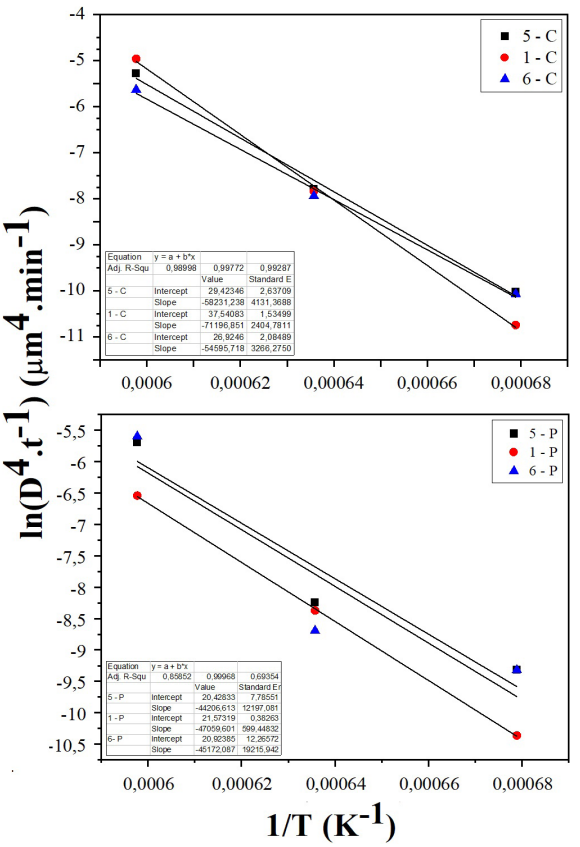

Figure 10. Arrhenius plot for the grain growth.

Table 3. Estimated grain growth activation energies.

Sample	Grain growth activation energy (Q, kJ/mol)
5 - C	484.2
1 - C	591.9
6 - C	453.9
5 - P	367.5
1 - P	391.3
6 - P	275.5

of the plot due to the change in the conduction mechanism, which generally starts at 500 °C [26]. The oxygen ionic conductivity of doped ceria materials can be explained as follows:

$$\text{At low temperatures: } \sigma = \frac{\sigma_0}{T} e^{\frac{-(\Delta H_m + \Delta H_a)}{kT}}, \tag{7}$$

$$\text{At high temperatures: } \sigma = \frac{\sigma_0}{T} e^{\frac{-(\Delta H_m)}{kT}}, \tag{8}$$

where ΔH_m is the migration enthalpy of the oxygen ions and ΔH_a is the association enthalpy of the dopant ion with the oxygen vacancies [27], k is the Boltzmann constant (8.617×10^{-5} eVK^{-1}), and T is temperature. For the cellulose templating method, calculated HT and LT activation energies are similar at 1200 and 1300 °C, but at 1400 °C, there is a significant

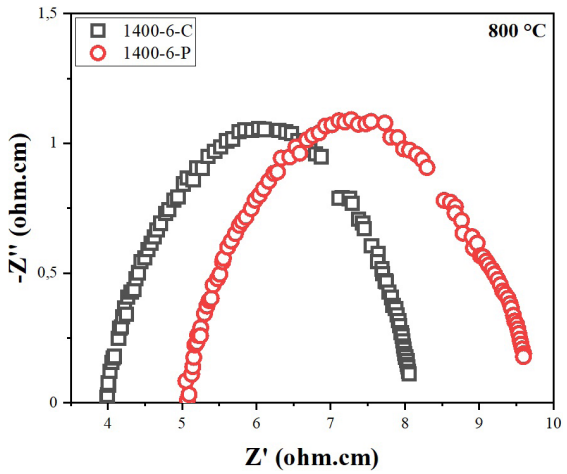

Figure 11. Impedance spectra of the CT and PVAT electrolytes measured at 800 °C.

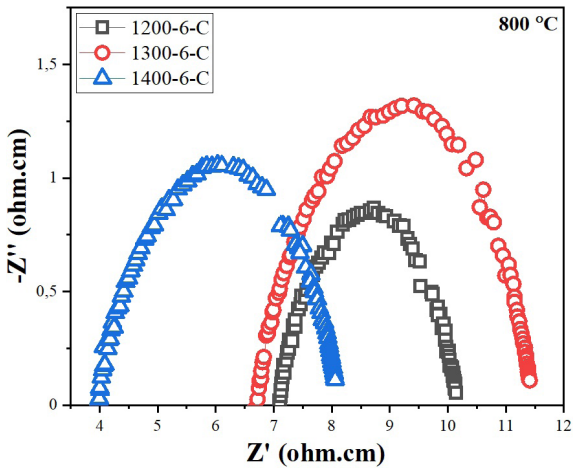

Figure 12. Impedance spectra of the samples prepared by cellulose templating method.

Table 4. EIS analysis results for the electrolytes prepared by the CT method.

Electrolyte	Total ionic conductivity (S cm^{-1}, 800 °C)	Area specific resistivity (cm S^{-1}, 800 °C)	E_A (high temperature, eV)	E_A (low temperature, eV)	ΔE (eV)
1200-6-C	0.030	33.333	0.872	0.892	0.020
1300-6-C	0.033	30.303	0.896	0.916	0.020
1400-6-C	0.050	20.000	0.742	0.829	0.087

decrease at both HT and LT activation energies. Consequently, the high ionic conductivity of the 1400–6-C electrolyte can be explained via decrease in the activation energy.

4. Conclusion

SDC20 electrolytes were successfully synthesized by the simple and fast cellulose templating and PVA templating methods and characterized by TGA/DTA, XRD, EIS, and SEM analysis. SDC20 powders with a single fluorite phase were obtained

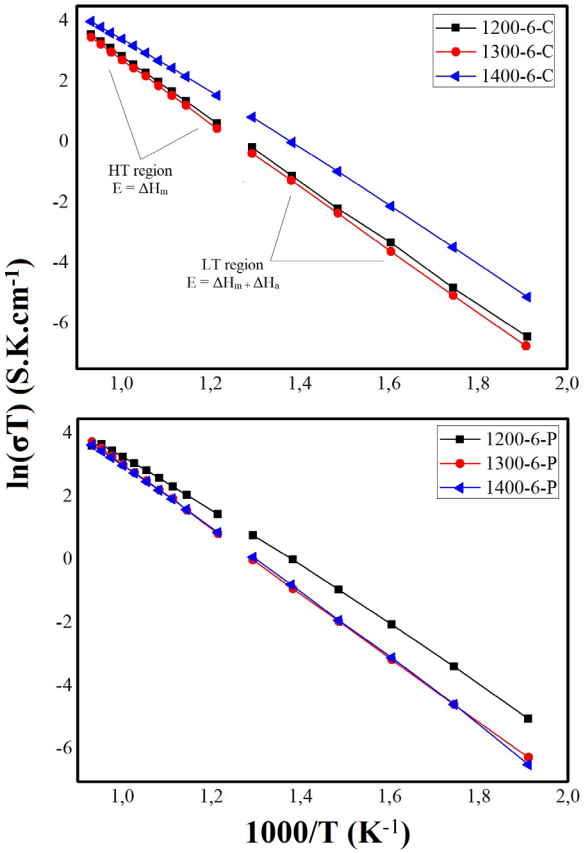

Figure 13. Arrhenius plots of the electrolytes.

after the calcination at 600 °C. Pellets were prepared with the CIP process and sintered at 1200–1400 °C temperature range for 5 min, 1 h, and 6 h each. A relative density of over 88% was reached in all samples. The grain growth kinetics is examined with SEM images. The average grain sizes were determined via the linear intercept method. The dominant diffusion mechanism was found to be the grain boundary diffusion and, the activation energy of the sintering was calculated. The highest ionic conductivity value (0.050 S cm^{-1}) was achieved for the 1400-6-C sample. The cellulose templating method is a more effective method to prepare mixed oxide structures than the precipitation and solid-state methods, as it provides higher performance electrolytes.

Acknowledgment
This work was supported by İstanbul University-Cerrahpaşa Research Fund [project no. 32459]; The Scientific and Technological Research Council of Turkey (TÜBİTAK) [project no. 216M509].

Conflict of interest
No potential conflict of interest was reported by the authors.

References

1. Kim KJ, Choi SW, Kim MY, Lee MS, Kim YS et al. Fabrication characteristics of SOFC single cell with thin LSGM electrolyte via tape-casting and co-sintering. Journal of Industrial and Engineering Chemistry 2016; 42: 69-74. doi: 10.1016/j.jiec.2016.07.041

2. Fuentes RO, Baker RT. Synthesis and properties of gadolinium-doped ceria solid solution for IT-SOFC electrolytes. International Journal of Hydrogen Energy 2008; 33: 3480-3484. doi: 10.1016/j.ijhydene.2007.10.026

3. Prasad DH, Son JW, Kim BK, Lee HW, Lee JH. Synthesis of nano-crystalline $Ce_{0.9}Gd_{0.1}O_{1.95}$ electrolyte by novel sol–gel thermolysis process for IT-SOFCs. Journal of the European Ceramic Society 2008; 28 (16): 3107-3112. doi: 10.1016/j.jeurceramsoc.2008.05.021

4. Godinho MJ, Gonçalves RF, Santos LPS, Varela JA, Longo E et al. Room temperature co-precipitation of nanocrystalline CeO_2 and $Ce_{0.8}Gd_{0.2}O_{1.9-\delta}$ powder. Materials Letters 2007; 61: 1904-1907. doi: 10.1016/j.matlet.2006.07.152

5. Zhu B, Liu X, Sun M, Ji S, Sun J. Calcium doped ceria-based materials for cost-effective intermediate temperature solid oxide fuel cells. Solid State Sciences 2003; 5: 1127-1134. doi: 10.1016/S1293-2558(03)00123-7

6. Ding D, Liu B, Zhu Z, Zhou S, Xia C. High reactive $Ce_{0.8}Sm_{0.2}O_{1.9}$ powders via a carbonate co-precipitation method as electrolytes for low-temperature solid oxide fuel cells. Solid State Ionics 2008; 179: 896-899. doi: 10.1016/j.ssi.2007.11.015

7. Li X, Feng Z, Lu J, Wang F, Xue M et al. Synthesis and electrical properties of $Ce_{1-x}Gd_xO_{2-x/2}$ (x = 0.05-0.3) solid solutions prepared by a citrate–nitrate combustion method. Ceramics International 2012; 38: 3203-3207. doi: 10.1016/j.ceramint.2011.12.025

8. Peng R, Xia C, Fu Q, Meng G, Peng D. Sintering and electrical properties of $(CeO_2)_{0.8}(Sm_2O_3)_{0.1}$ powders prepared by glycine–nitrate process. Materials Letters 2002; 56: 1043-1047.

9. Chen W, Li F, Yu J. Combustion synthesis and characterization of nanocrystalline CeO_2-based powders via ethylene glycol–nitrate process. Materials Letters 2006; 60: 57-62. doi: 10.1016/j.matlet.2005.07.088

10. Li S, Ge L, Gu H, Zheng Y, Chen H et al. Sinterability and electrical properties of ZnO-doped $Ce_{0.8}Y_{0.2}O_{1.9}$ electrolytes prepared by an EDTA-citrate complexing method. Journal of Alloys and Compounds 2011; 509: 94-98. doi: 10.1016/j.jallcom.2010.08.111

11. Sarıboğa V, Özdemir H, Öksüzömer MAF. Cellulose templating method for the preparation of $La_{0.8}Sr_{0.2}Ga_{0.83}Mg_{0.17}O_{2.815}$ (LSGM) solid oxide electrolyte. Journal of the European Ceramic Society 2013; 33:1435-1446. doi: 10.1016/j.jeurceramsoc.2013.01.016

12. Ma J, Jiang C, Zhou X, Meng G, Liu X. Polyvinyl alcohol-induced low temperature synthesis of CeO_2-based powders. Journal of Power Sources 2006; 162: 1082-1087. doi: 10.1016/j.jpowsour.2006.07.050

13. Sifontes AB, Gonzalez G, Ochoa JL, Tovar LM, Zoltan T et al. Chitosan as template for the synthesis of ceria nanoparticles. Materials Research Bulletin 2011; 46: 1794–1799. doi: 10.1016/j.materresbull.2011.07.049

14. Güçtaş D, Sarıboğa V,Öksüzömer MAF. Preparation of $Sm_{0.2}Ce_{0.8}O_{1.9}$ electrolytes via the chitosan templating method and investigation of the sintering behavior. Journal of Asian Ceramic Societies 2021; 9 (2); 487-497, doi: 10.1080/21870764.2021.1891686

15. Özdemir H, Sarıboğa V, Öksüzömer MAF, Gürkaynak MA. Preparation and characterization of Ca-Sm-Ce mixed oxides via cellulose templating method for solid oxide fuel cell applications. Journal of Power Sources 2012; 219: 155-162. doi: 10.1016/j.jpowsour.2012.07.033

16. Jiang C, Ma J, Liu X, Meng G. Electrochemical performance of a solid oxide fuel cell based on $Ce_{0.8}Sm_{0.2}O_{2-\delta}$ electrolyte synthesized by a polymer assisted combustion method Journal of Power Sources 2007; 165: 134-137. doi: 10.1016/j.jpowsour.2006.12.026

17. Yang H, Xu S, Jiang L, Dan Y. Thermal decomposition behavior of poly (vinyl alcohol) with different hydroxyl content. Journal of Macromolecular Science, Part B 2012; 51 (3): 464-480. doi: 10.1080/00222348.2011.597687

18. Dutta SK, Sprigge RM. Grain growth in fully dense ZnO. Journal of the American Ceramic Society 1970; 53 (1): 61–62.

19. Le S, Zhu S, Zhu X, Sun K. Densification of $Sm_{0.2}Ce_{0.8}O_{1.9}$ with the addition of lithium oxide as sintering aid. Journal of Power Sources 2013; 222: 367-372. doi: 10.1016/j.jpowsour.2012.08.020

20. Rahaman MN. Seramic processing and sintering. New York: Marcel Dekker, Inc, 1995.

21. Marrero-Lopez D, Martin-Sedeno MC, Pena-Martinez J, Ruiz-Morales JC, Nunez-Coello P et al. Microstructure and conductivity of $La_{1-x}Sr_xGa_{0.8}Mg_{0.2}O_{3-\delta}$ electrolytes prepared using the freezedrying method. Journal of the American Ceramic Society 2011; 94 (4): 1031-1039.

22. Zhang T, Hing P, Huang H, Kilner J. Sintering and grain growth of co-doped CeO_2 ceramics. Journal of the European Ceramic Society 2002; 22 (1): 27-34. doi: 10.1016/S0955-2219(01)00240-0

23. Nieh TG, Wadsworth J. Superelastic behaviour of a fine-grained, yttria-stabilized, tetragonal zirconia polycrystal (Y-TZP). Acta Metallurgica et Materialia 1990; 38 (6):1121-1133. doi: 10.1016/0956-7151(90)90185-J

24. Jaiswal N, Upadhyay S, Kumar D, Parkash O. Sm^{3+} and Sr^{2+} co-doped ceria prepared by citrate-nitrate auto-combustion method. International Journal of Hydrogen Energy 2014; 39: 543-551.doi:10.1016/j.ijhydene.2013.10.009

25. Spiridigliozzi L, Dell'Agli G, Marocco A, Accardo G, Pansini M et al. Engineered co-precipitation chemistry with ammonium carbonate for scalable synthesis and sintering of improved $Sm_{0.2}Ce_{0.8}O_{1.90}$ and $Gd_{0.16}Pr_{0.04}Ce_{0.8}O_{1.90}$ electrolytes for IT-SOFCs. Journal of Industrial and Engineering Chemistry 2018; 59: 17-27. doi: 10.1016/j.jiec.2017.10.001

26. Tianshu Z, Hing P, Huang H, Kilner J. Ionic conductivity in the CeO_2-Gd_2O_3 system ($0.05 \leq Gd/Ce \leq 0.4$) prepared by oxalate coprecipitation, Solid State Ionics 2002; 148: 567-73. doi: 10.1016/S0167-2738(02)00121-2

27. Omar S, Wachsman ED, Jones JL, Nino JC. Crystal structure-ionic conductivity relationships in doped ceria systems. Journal of the American Ceramic Society 2009; 92 (11): 2674-2681. doi: 0.1111/j.1551-2916.2009.03273